Electronic Supplementary Information

Tailored ultra-small Prussian blue-based nanoparticles for MRI imaging and combined photothermal/photoacoustic theranostics

Lucile Fétiveau,[a] Gabriella Paul,[a] Alba Nicolas-Boluda,[b] Jeanne Volatron,[b] Riya George,[a] Sophie Laurent,[c] Robert Muller,[c] Lucie Sancey, [d] Philippe Mejanelle,[e] Alexandre Gloter,[f] Florence Gazeau[b] and Laure Catala [a]*

Instrumentation

Dynamic Light Scattering (DLS) and zeta potential

The two types of measurements were performed on a Nanozetasizer (equipped with backscattering mode) from Malvern. The hydrodynamic diameter of particles or aggregates of particles were estimated using volume profiles.

TEM

TEM micrographs were acquired using a JEOL 1400 under a voltage of 120 keV and CCD camera Orius SC 1000A2. Particles were deposited on Formvar-coated copper grids.

X-Ray Powder Diffraction (XRPD)

XRPD was carried out on powders with a Philips Panalytical X'Pert Pro MPD powder diffractor equipped with a fast detector using Cu K_α . Each measurement was acquired overnight.

Fourier-transform Infrared spectroscopy (FT-IR)

FT-IR spectra were registered on a Perkin Elmer Spectrum 100. KBr pellets, containing 1 mg of ground samples, were used to perform the measurement in transmission mode between 4000 and 200 cm^{-1}.

Inductively Coupled Plasma-Optical Emission spectroscopy (ICP-OES)

ICP-OES analysis were performed with a Thermo ICAP 6500 system using the axial configuration. The operating parameters were as follows: RF power: 1150 W; Ar cooling gas flow 12 $L.min^{-1}$; Ar auxiliary gas flow 0.5 $L.min^{-1}$ and Ar nebulizer gas flow 0.5 $L.min^{-1}$.

Elemental Analysis

The dextran content was assessed by determination of C,H,N content contained in the powders by combustion analysis in ICSN-CNRS Gif sur Yvette center.

Relaxivity measurements (T_1 and T_2)

Measurements of T_1 and T_2 relaxation times were performed at 37°C and 5°C on a Bruker Minispec mq20, mq60 and on an Avance 300 spectrometer (Karlsruhe, Germany) working at 20, 60 and 300 MHz (0.47, 1.41, 7 T respectively).
^{1}H NMRD profiles (Nuclear Magnetic Resonance Dispersion) were performed at 37°C with Stelar fast field cycling relaxometer (Mede, Italy) over a range of magnetic fields extending from 0.01 to 40 MHz.

Photothermal Efficiency

Colloidal suspensions of the particles were irradiated with a 808 nm laser delivered by an optical fiber with a power of 1 W.cm^{-2} for 3 min. The distance between the optical fiber and sample was fixed in order to irradiate all the same surface. A blank was first registered to check that pure water revealed no heating under these conditions.

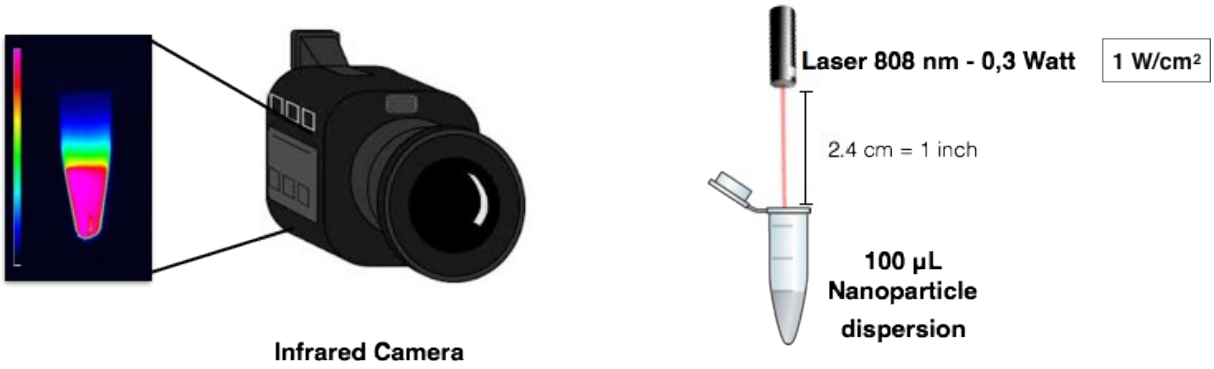

Synthesis

Synthesis of $K_{4y-3+x}Gd^{III}_xY^{III}_{1-x}[Fe^{II}(CN)_6]_y$, nH_20 with Y = In or Fe

After cooling down at 2°C, 100 mL of an aqueous solution containing $GdCl_3,6H_2O$ and $InCl_3,xH_2O$ or $Fe(NO_3)_3,9H_2O$ (0.5 mM) was added rapidly in an aqueous solution of $K_4Fe(CN)_6$ (100 mL at 0.5 mM) under vigorous stirring. The mixture was left under stirring at 2°C during 30 minutes and at room temperature for 30 minutes. At this step, dynamic light scattering (DLS) was used to check the hydrodynamic diameter of particles and zeta potential was evaluated.

Coating with dextran

To the solution described above, 25 equivalents of the dextran monomer (using dextran Low fraction from Aldrich) with respect to Fe^{II} were added. To recover the particles, 0.8 equivalent in volume of acetone with respect to the volume of the colloidal suspension was added. After centrifugation (8000 rpm) for 15 minutes, powder was dried under vacuum. The resulting powders were characterized by FT-IR, TEM, XRPD, ICP measurements and elemental analysis. Purification of nanoparticles may alternatively be done without addition of acetone by dialysis or by ultrafiltration and post-washing with water.

Coating with Polyvinylpyrrolidone (PVP)

100 equivalents of the PVP monomer (using PVP MW=40 000 g.mol^{-1}) were added into the fresh colloidal solution of nanoparticles. Before centrifugation and vacuum drying, particles were flocculated by addition acetone (3 times the volume of the colloidal solution). Powders were analyzed by FT-IR, TEM, XRDP, ICP measurements and elemental analysis.

Dispersion of $K_{4y-3+x}Gd^{III}_{x}Y^{III}_{1-x}[Fe^{II}(CN)_6]_y$, nH_20 @ Dextran or PVP nanoparticles with Y = In or Fe

Powders of particles were dispersed in water at 10 mM or 1 mM (of nanoparticles). The solution obtained was sonicated during 5 minutes. The size of particles in dispersion was evaluated by DLS and TEM. Measurement of relaxation times (T_1 and T_2), NMRD profiles and T_1-weighted contrasts in MRI were performed using these dispersions.

Figure S1
Transmission Electronic Microscopy images for GdInFe@dextran nanoparticles with 5%, 10%, 15%, 25%, 50%, 75% and 100% of GdIII.

TEM micrographs of the dispersions obtained in water. Arrows show the presence of KGdFe particles.

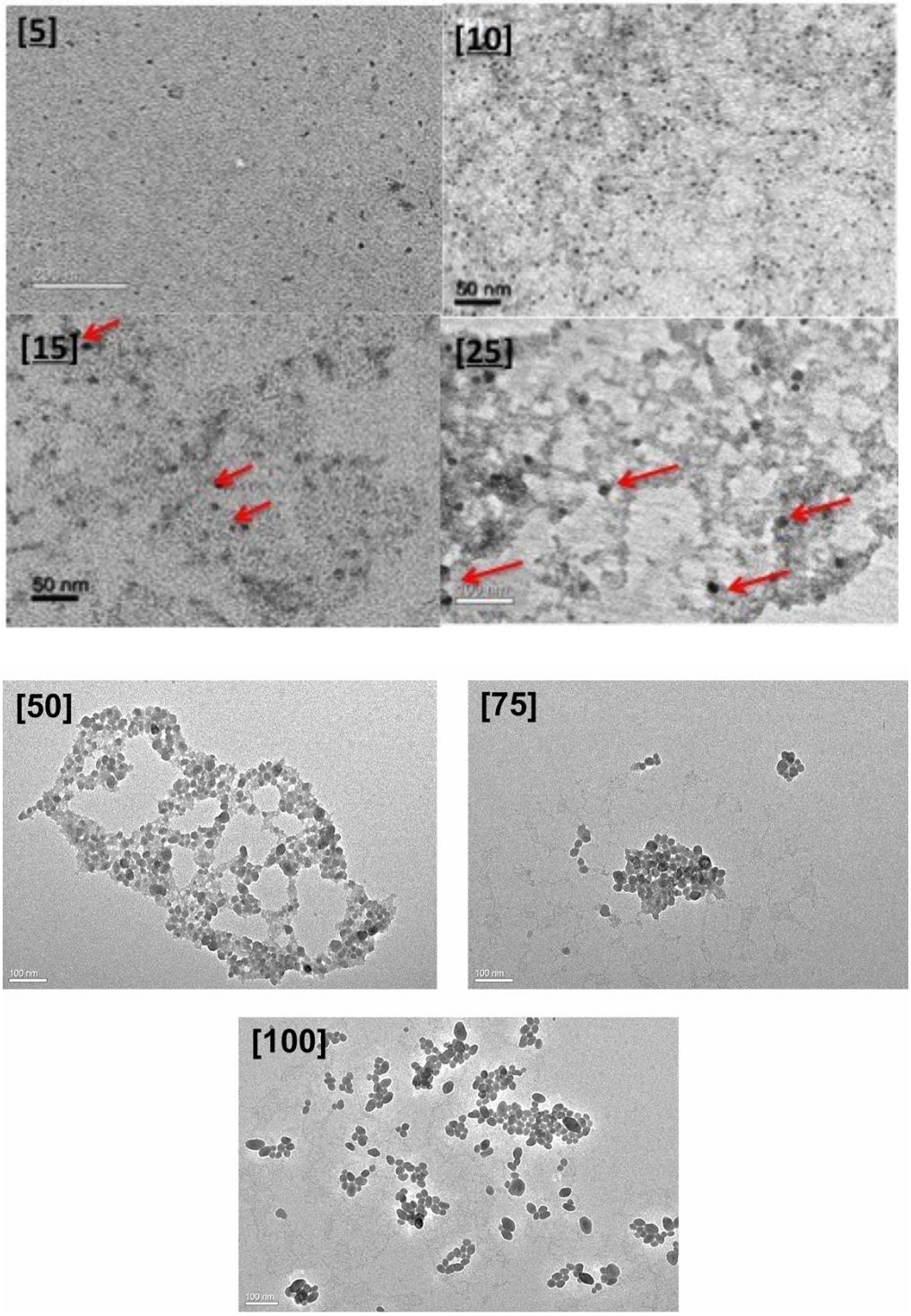

TEM image of GdFeFe@dextran [10]

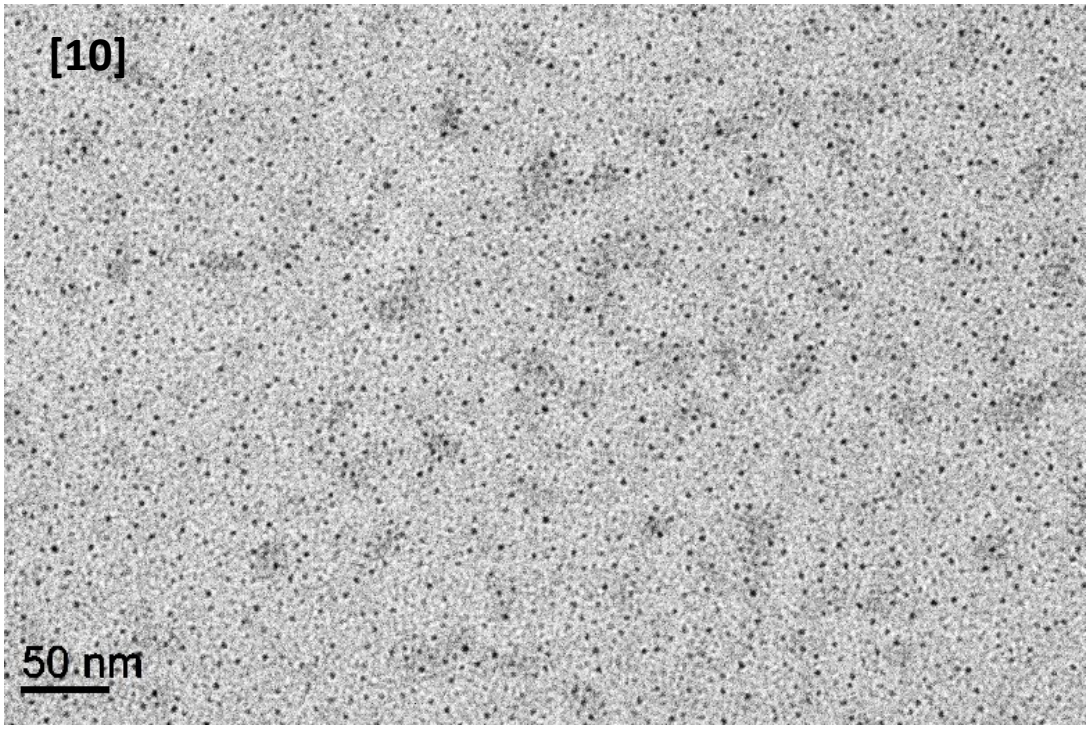

Figure S2
X-Ray powder diffractograms of GdInFe[x] @dextran nanoparticles

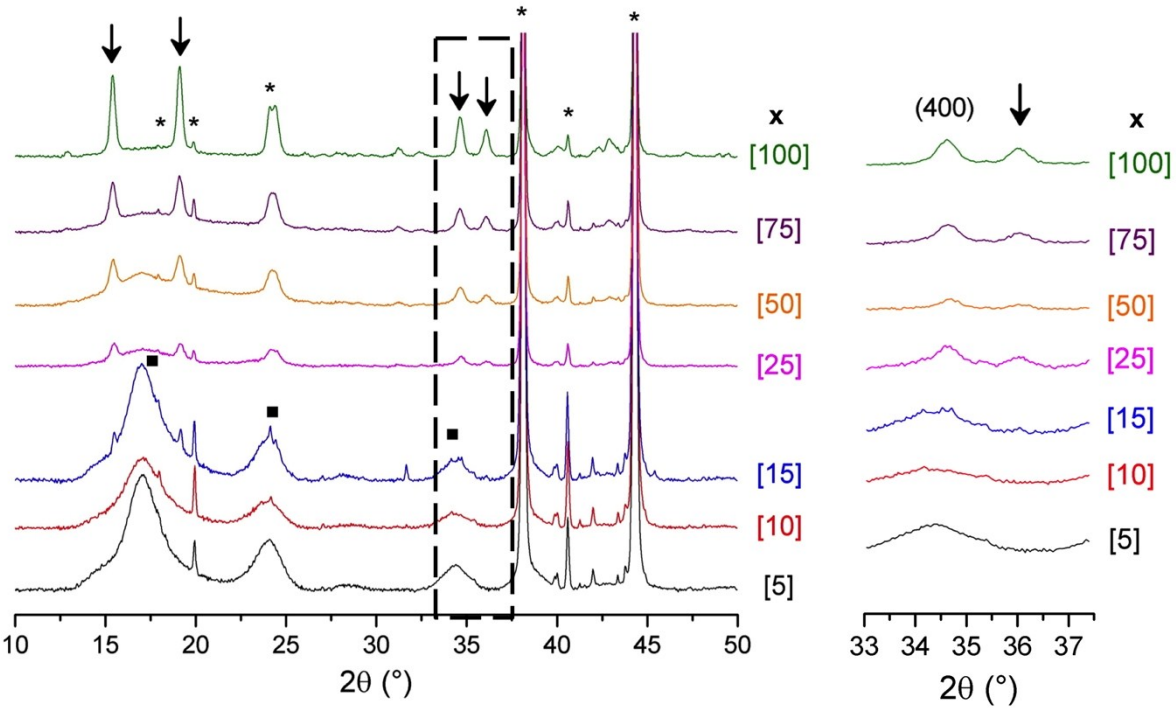

Arrows indicate the reflections of the $KGd^{III}[Fe^{II}(CN)_6]$ orthorhombic structure
Squares indicate the reflections to the $In^{III}[FeII(CN)_6]_{3/4}$ fcc structure
Asterisks correspond to the aluminium holder.

Figure S3
X-Ray powder diffractograms, cell parameter and correlation length dependence over the Gd(III) content, extracted from X-Ray powder diffractograms of GdInFe@dextran and GdFeFe@dextran (*= holder)

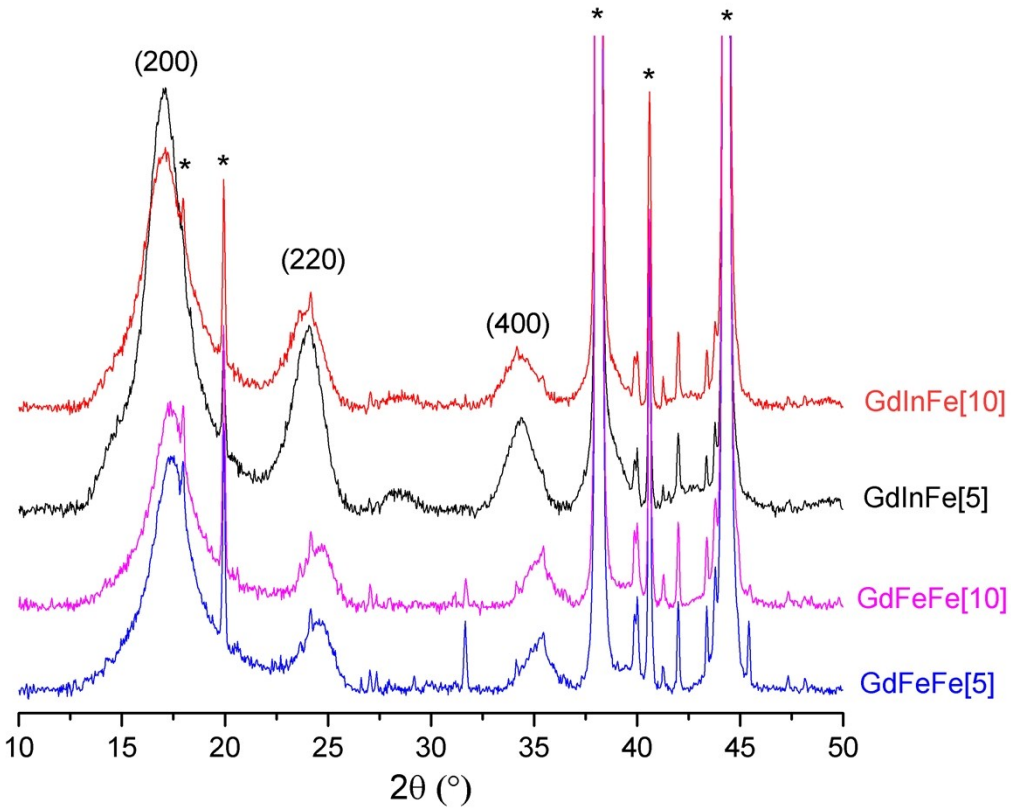

Nanoparticles	d (nm)	a (Å)
GdInFe [5]	5.0±0.5	10.44 ±0.03
GdInFe [10]	5.1±0.5	10.45±0.03
GdFeFe [5]	4.4±0.5	10.15±0.03
GdFeFe [10]	4.2±0.5	10.15±0.03

To calculate cell parameter (a) and crystalline domain size (d) for each sample, Scherrer formula and Bragg law were respectively used on (220) and (400) Bragg reflection peaks.
The cell decrease observed between GdInFe and GdFeFe particles is due to smaller ionic radius of Fe^{III} (0.55 Å) compared to In^{III} (0.8 Å). Besides, cell parameter is coherent with cell parameter of $InFe_{0,75}$ PBA (10.45 Å) for GdInFe particles and with Prussian Blue (10.17 Å) for GdFeFe particles. This suggests a PBA core with coordinated Gd^{III}-NC-Fe^{II} pairs at the surface of the particles.

Figure S4

Dynamic Light Scattering plots (in volume) depending on GdIII content at the end of the synthesis (red) and with dextran coating after redispersion in H2O (black)

a) *For [GdInFe]= 10 mM*

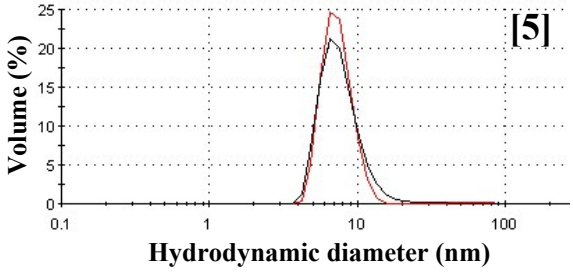

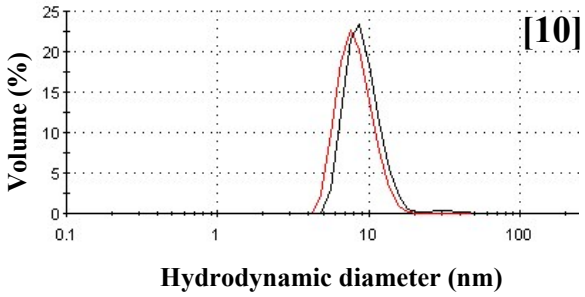

b) *For [GdFeFe] = 1 mM*

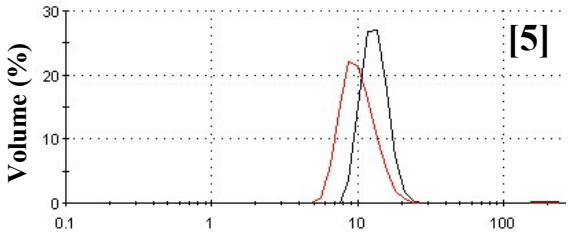

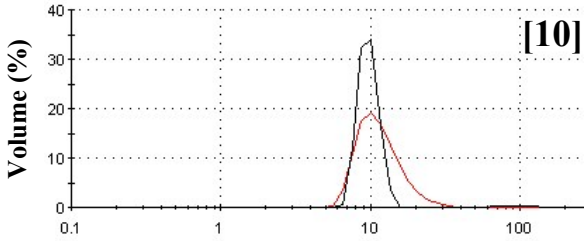

Figure S5
Zeta potential of nanoparticles with dextran coating after redispersion in H2O

a) For [GdInFe]= 10 mM

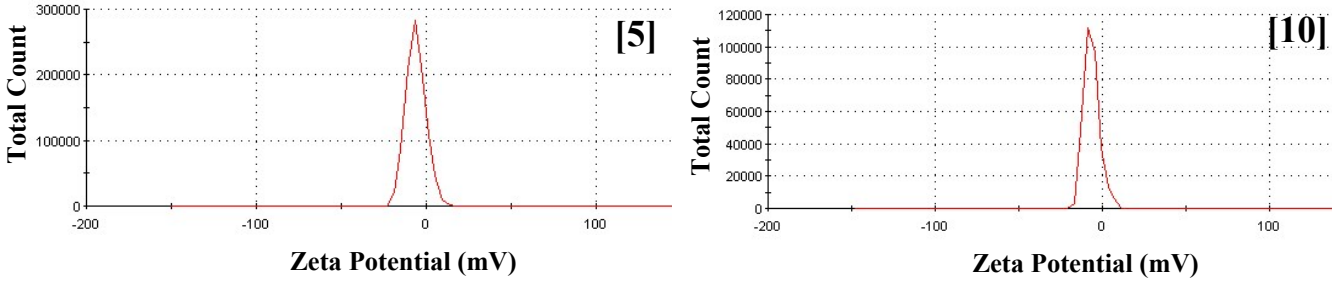

b) For [GdFeFe] = 1 mM

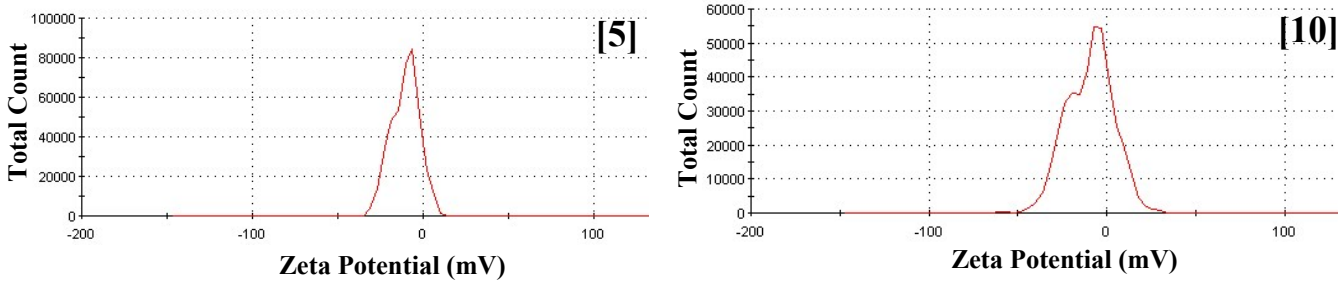

Figure S6
FT-Infra-red spectra of GdYFe@dextran (Y=In or Fe) for different GdIII contents; Zoom on the 2300-1900 cm-1 and 700-400 cm-1 ranges.

a) GdInFe@dextran

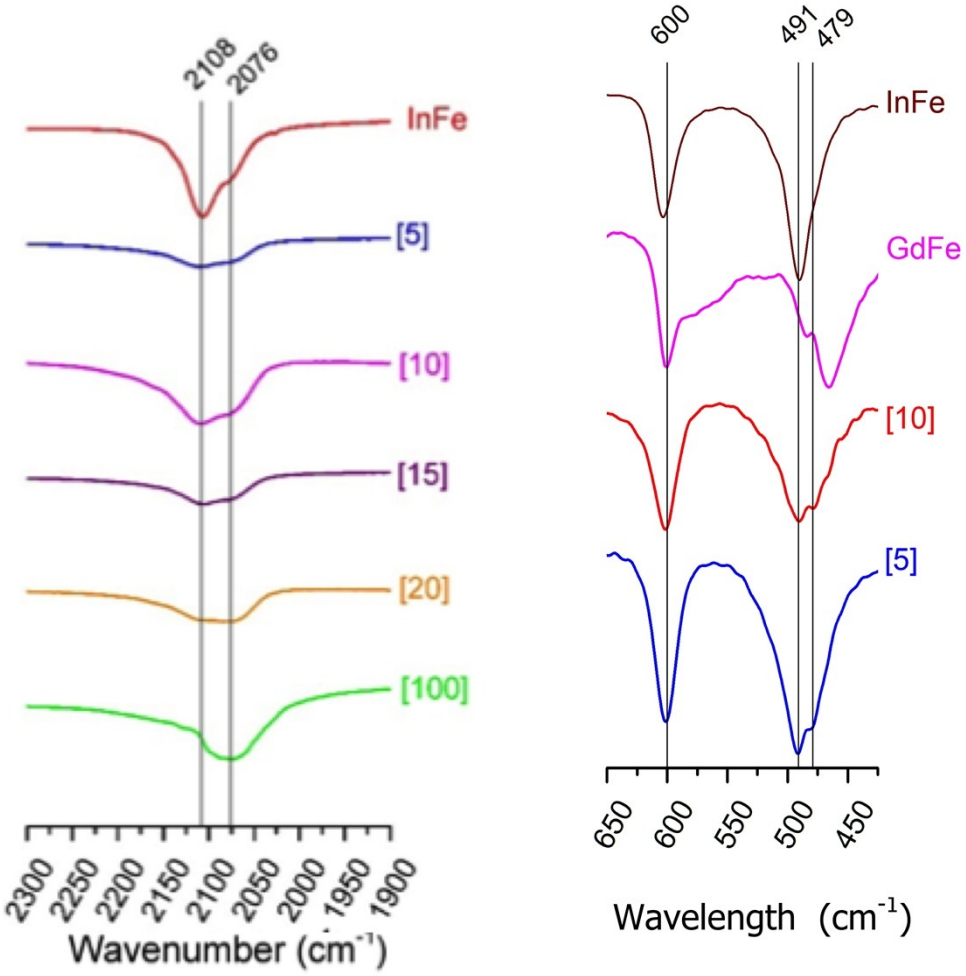

b) GdFeFe@dextran

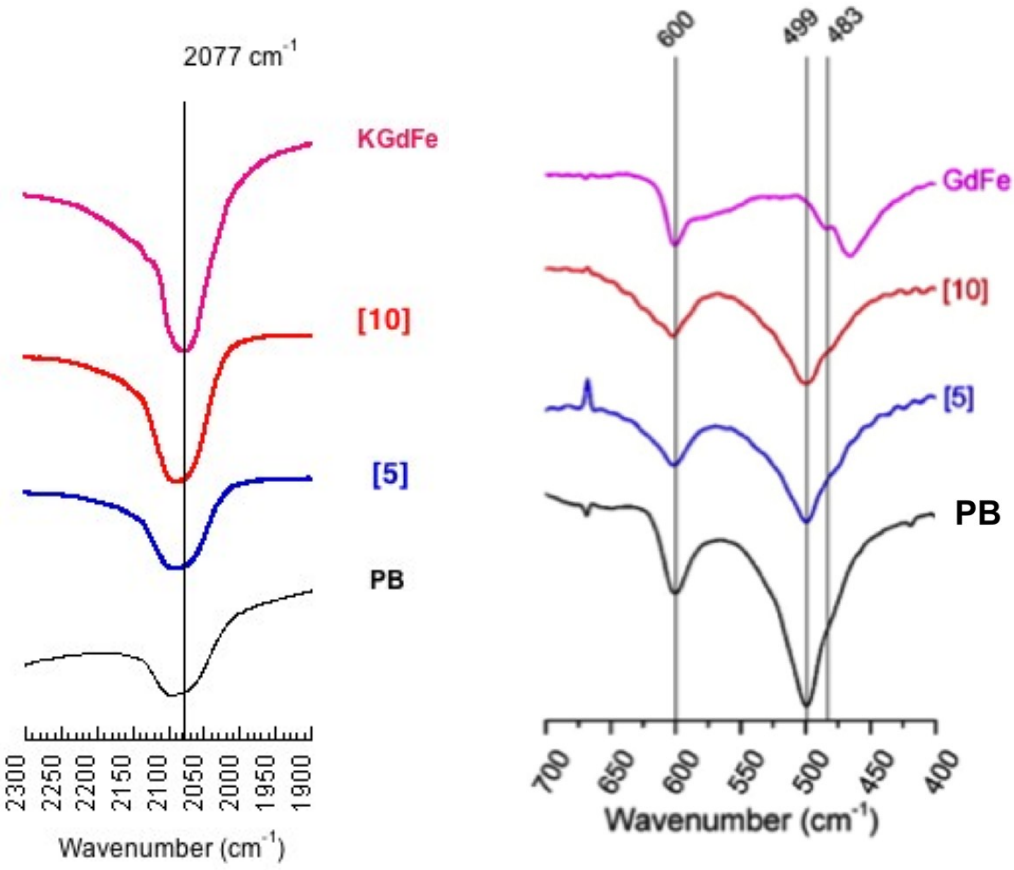

STEM-EELS experiments

STEM (scanning transmission electron microscope) experiments have been performed in a modified VG-HB5 equipped with a cryo sample holder cool down at 150 K. EELS (electron energy loss) spectra was collected using a modified GATAN EELS spectrometer equipped with an electron multiplying CCD (EM-CCD) as a final detector. Low temperature helps to avoid damage and to remove any contamination problem, notably during the EELS measurements that require longer pixel acquisition times (ca. 10 ms). The EM-CCD helps to maintain a good signal to noise ratio at lower counting rate.

Spectro-microscopy with typical 2 nanometres resolution have been performed with an energy range spanning from ca. 100 eV to ca 800 eV. It comprises the Gd-N (140 eV), C-K (285 eV), N-K (401 eV), In-M (443 eV), O-K (530 eV), and Fe-L (710 eV) edges.

The figure S7-a show the STEM-HAADF (high angle annular dark field) collected before the STEM-EELS spectromicroscopy. The green box indicated the area for the STEM-EELS measurement. The figure S7-b compared the raw EELS data extracted from a 5 nm particle and off the particle. Both edges exhibit a very intense C-K edge due to the supporting carbon layer. Metals edges from the PBA particle only appear with a small intensity but a Fe-L edge is clearly visible for the spectrum on the particle. The figures S7-c show the HAADF obtained during the STEM-EELS experiment along with the Fe, Gd and C maps. The maps have been obtained through a conventional A.E-r background removal technique. Despite the small amount of Fe and Gd atoms, both elements can be detected by EELS due to the large cross section and the quite narrow shape of the Fe-L and Gd-N edges. On the other hand, indium and nitrogen cannot be mapped through a conventional EELS mapping technique.

Spectral unmixing have thus been done, using vertex component analysis (VCA) [Dobigeon 2012]. The obtained results for the 2 main components are exhibited in figure S8. Due to the unmixing procedure, the components have a better signal to noise ratio as compared to spectra extracted from individual particle or nanometre scale regions. The retrieved component 1 can be associated to the PBA particles as it can be derived from its spatial distribution. The component 2 corresponds mostly to the supporting film. The component 1 exhibits clearly the EELS signal for Gd, N, In and Fe. The VCA unmixing clearly demonstrated the concomitant presence of these elements in each nanoparticle.

Due to the small amount of metals (Gd, In, Fe), the presence of a carbon film, the spatial drift associated with the cryo holder and the limited resolution of the VG microscope, it was not possible to investigate the Gd distribution within each nanoparticles.

Dobigeon N., Brun N., Blind Linear unmixing of EELS spectrum-images, ULTRAMICROSCOPY 120 : 25-34 JUN 2012

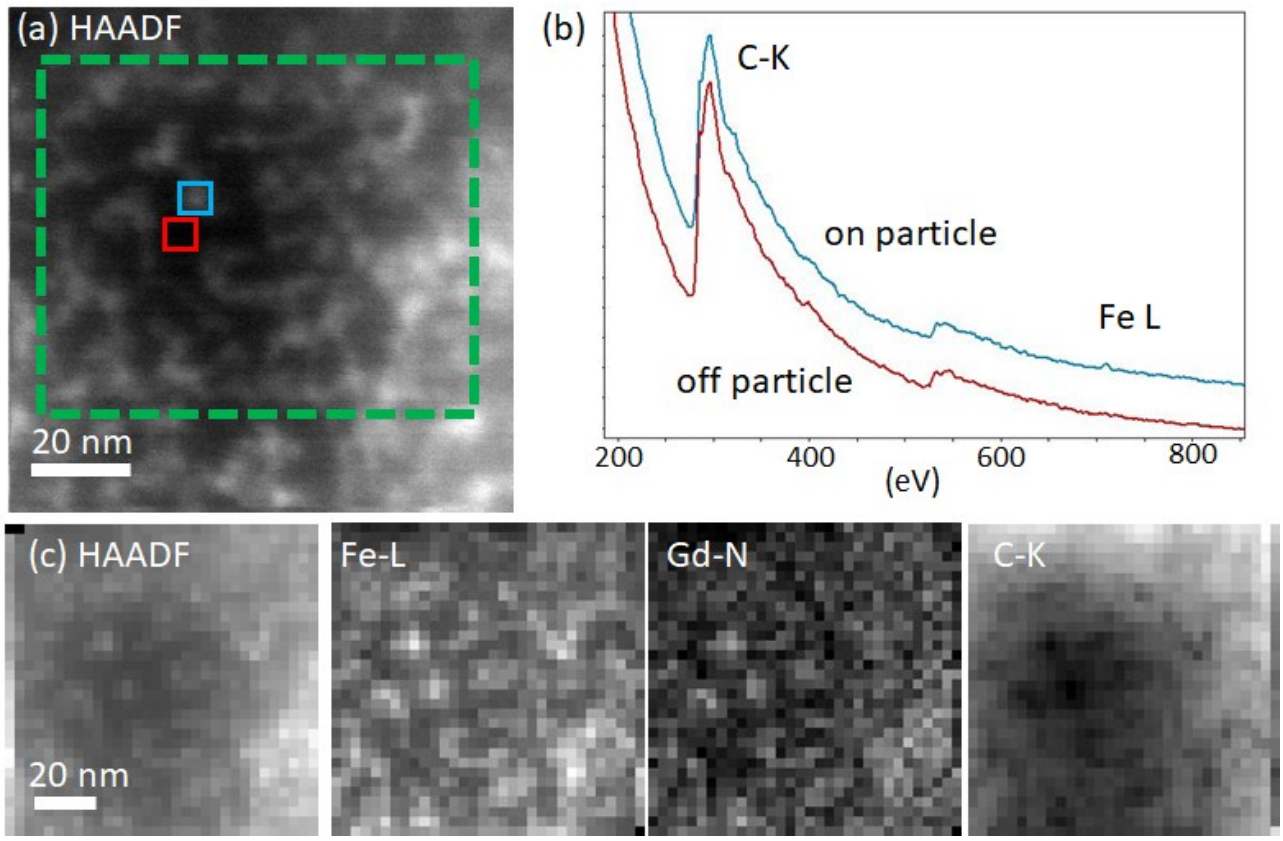

Figure S7 STEM-EELS chemical mapping of the PBA particle. (a) HAADF image, (b) raw EELS spectra on and off a PBA particle, (c) chemical map and corresponding HAADF.

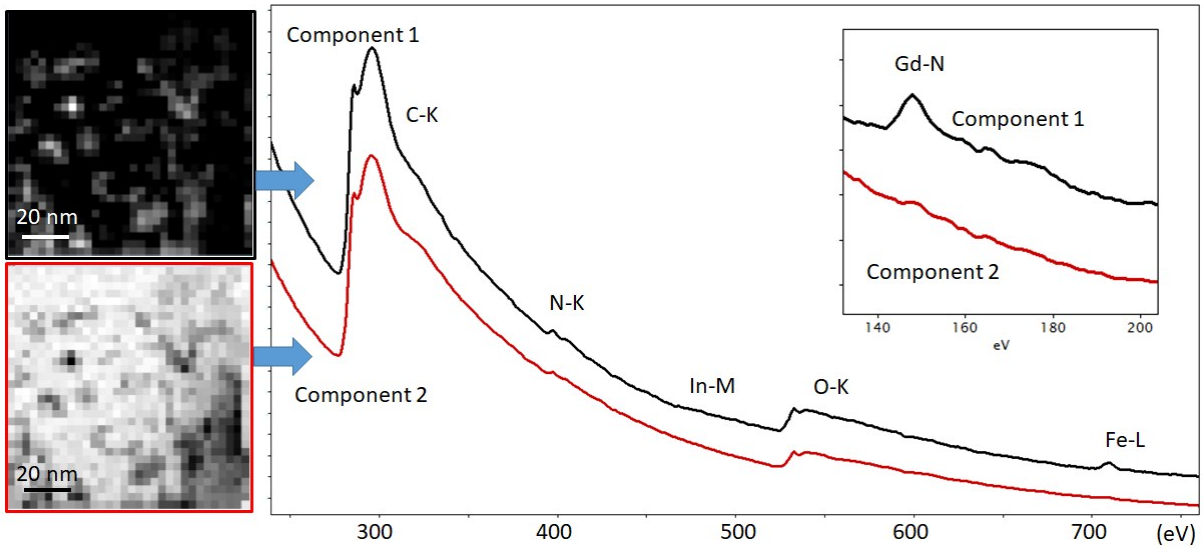

Figure S8 Spectral unmixing with a Vertex Component Analysis (VCA). The main 2 components are visible along with their spatial distribution. The component 1 comprises Gd, N, In and Fe edges and correspond to the PBA nanoparticules.

Elemental analysis; Chemical composition and leaching

Ultrafiltration method

The powders of GdYFe[x]@dextran (Y = In^{III} or Fe^{III}) were dispersed in 1 mL of H_2O with a concentration of nanoparticles of 0.2 mM. Colloidal solutions were centrifuged during 30 min at 8000 rpm in Vivaspin 6 with PES (polyether sulfone) membrane 5000 MWCO. The ultrafiltrate was washed with an equivalent volume of water and then centrifuged in the same conditions.
The filtrate was analyzed by ICP-OES after dilution in HNO_3 at 10^{-2} M to determine the quantity of Gd, In and Fe released.

Calculation of quantity of free Gd, In and Fe

The chemical compositions of all batches of nanoparticles were analysed by ICP-OES. Metal contents in particles were evaluated on dispersions of powders in HNO_3 10^{-2} M. Knowing the quantity of powder weighted and dilution factor to prepare the filtrate, the total amount of Gd, In and Fe in dispersion were determined. By ICP measurement on filtrates, the leaching of each metal (Gd, In or Fe) was estimated.

$$\text{Leaching of metal M (\%)} = \frac{[M]_{dispersion}}{[M]_{filtrate}} \times 100$$

With $[M]_{dispersion}$: concentration of metal in dispersion before filtration
$[M]_{filtrate}$: concentration of metal in filtrate after filtration

Xylenol Assay

The orange xylenol assay was used to estimate the proportion of free Gd^{III} according to Orange xylenol is an organic compound that can form complexes with free Gd3+ ions. Complexation with Gd^{III} leads to a colorimetric shift towards violet. The quantification of free Gd^{III} should be done at a constant pH. The solutions used for the assay are prepared in an acetate buffer solution at pH = 5.8. The first step of the assay is to establish a calibration curve. For this, a standard solution for ICP of Gd^{III} ([Gd] = 1000 $mg.L^{-1}$ = 6.36 M) is used as stock solution. Five standard solutions are prepared, as reported in the table below.

[Gd] ($mg.L^{-1}$)	0,2	0,5	1	2	3	4
[Gd] (µM)	1,27	3,18	6,36	12,7	19,1	25,4
Mother Solution	4 ppm	Standard	Standard	Standard	Standard	Standard
V_{total}(mL)	100	100	100	100	100	100
$V_{Mother\ solution}$(mL)	5	0,05	0,1	0,2	0,3	0,4

From the fit of the calibration line and the A_{573} / A_{433} ratios corresponding to absorbance at 573 nm and 433 nm, free Gd^{III} concentrations are determined in the samples.

UV visible spectra of standard solutions and Calibration curve

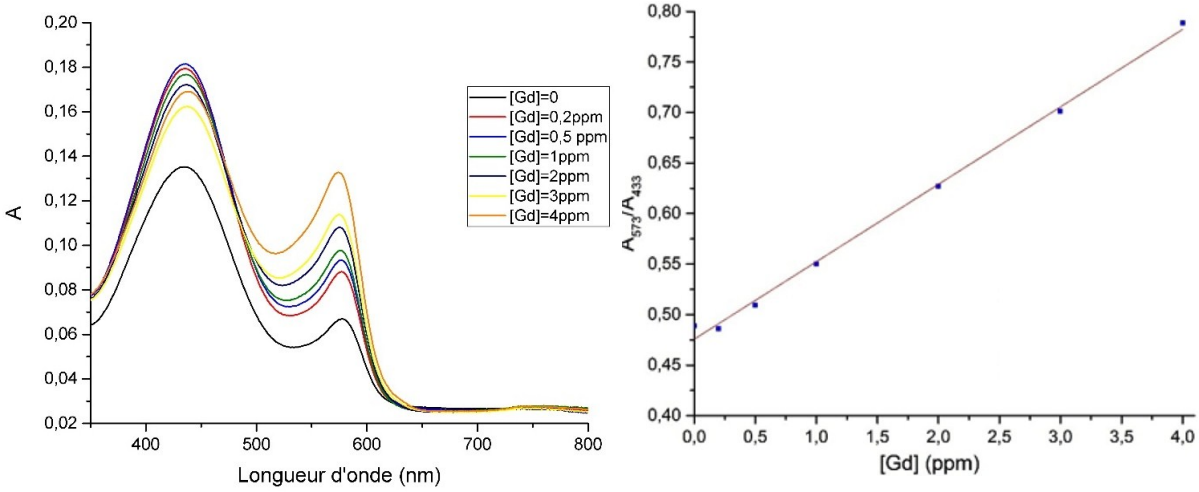

The equation of linear fitting of calibration curve is

$$\frac{A_{573}}{A_{433}} = 0{,}077\,[Gd] + 0{,}476$$

The analyses are carried out after ultrafiltration of the redispersed particles either in water or in the Fœtal Bovine Serum (FBS) and reported below.

Table S9 Quantity of free Gd^{III}, In^{III} and Fe^{II} determined by ICP and xylenol assay

BY ICP

Samples	GdIII		In^{III}		Fe	
	$mg.L^{-1}$ (ppm)	%	$mg.L^{-1}$ (ppm)	%	$mg.L^{-1}$ (ppm)	%
$Gd^{III}In^{III}Fe$ [5]	0.02	0.5	0.002	0.0006	0.04	0.03
$Gd^{III}In^{III}Fe$ [10]	0.03	1.3	0.0005	0.004	0.05	1.06
$Gd^{III}Fe^{III}Fe$[5]	0.15	6.2			0.07	0.26
$Gd^{III}Fe^{III}Fe$[10]	0.17	8.6			0.07	0.57

BY XYLENOL ASSAY

Samples	$[Gd^{III}]$ (ppm)	$[Gd^{III}]$ (µM)	% of free Gd^{III}
$Gd^{III}Fe^{III}Fe^{II}$[5]@$(dextran)_{25}$ in H_2O	0,5	3,2	3,1
$Gd^{III}Fe^{III}Fe^{II}$[5]@$(dextran)_{25}$ in FBS-t=1h	0,9	5,7	5,5
$Gd^{III}Fe^{III}Fe^{II}$[5]@$(dextran)_{25}$ in FBS-t=4h	0,8	5,1	5,2
$Gd^{III}Fe^{III}Fe^{II}$[5]@$(dextran)_{25}$ in FBS-t=24h	0,7	4,5	4,5

Table S10

Composition determined by Elemental Analysis and ICP:
($C_6H_{10}O_5$) stands for the dextran monomer

Sample Name	Composition
GdInFe [5]	$K_{0.4}Gd_{0.05}In_{0.95}[Fe(CN)_6]_{0.85}.38\ H_2O.(C_6H_{10}O_5)_{33}$
GdInFe[10]	$K_{0.32}Gd_{0.09}In_{0.91}[Fe(CN)_6]_{0.83}.34\ H_2O.(C_6H_{10}O_5)_{30}$
GdFeFe [5]	$K_{0.60}Gd_{0.06}Fe^{III}_{0.94}[Fe(CN)_6]_{0.90}.33\ H_2O.(C_6H_{10}O_5)_{26}$
GdFeFe [10]	$K_{0.60}Gd_{0.11}Fe^{III}_{0.89}[Fe(CN)_6]_{0.90}.37\ H_2O.(C_6H_{10}O_5)_{29}$

Explanation of the influence of Gd^{III} and Fe^{III} on the relaxivities of Table 1

The synthesized particles containing 5% and 10% Gd^{III} have very high values of relaxivities, of the order of 40 $mM^{-1}.s^{-1}$ for the diamagnetic core and between 46 and 55 $mM^{-1}.s^{-1}$ for the paramagnetic core. In order to better understand these observations, we took into account the contribution of Fe^{III} ions to the relaxivity that we had neglected in a first approximation.
To do so, we calculated the number of surface atoms and the proportion of GdIII and FeIII atoms at the surface. Calculations are shown in Table II-20.

% Gd^{III}	%Fe^{III}	Taille (nm)	N_T	N_S	N_S (Gd^{III})	N_S (Fe^{III})
6	94	4	365	194	22	172
11	89	4	365	194	40	154

Estimation of total number of atoms (N_T) and those located at the surface (N_s) of each particle and number of surface atoms of Gd^{III} and Fe^{III}.

Our model is based on the hypothesis that mainly the atoms located at the surface are participating actively to the relaxivity of the NPs.
The Fe^{3+} surface ion relaxivity was determined from measurements made on PB 4 nm particles and is 1.2 $mM^{-1}.s^{-1}$.
A relaxivity of 40 $mM^{-1}.s^{-1}$ per Gd^{III} was estimated form this study on GdInFe particles.. The particle's total relaxivity is calculated using the number of surface Gd^{III} is multiplied by 40 $mM^{-1}.s^{-1}$ and adding the number of surface Fe^{III} by 1.2 $mM^{-1}.s^{-1}$.

% Gd^{III}	N_S (Gd^{III})	r_1/Gd^{III}_s	r_1/part (Gd^{III}_s)	N_S (Fe^{III})	r_1/Fe^{III}_s	r_1/part (Fe^{III}_s)	r_1/part (Gd^{III}_s+ Fe^{III}_s)	% de r_1 (Gd^{III}_s)	% de r_1 (Fe^{III}_s)
6	22	40	876	172	1,2	206,5	1082,5	81	19
11	40	40	1606	154	1,2	184,6	1790,6	90	10

The sum of these two relaxivities gives the total relaxivity per particle. When considering only the participation of Gd^{III}, this would be equivalent to dividing this total relaxivity by the total number of Gd^{III} only (and not considering Fe^{III}). We hence find values of

50 $mM^{-1}.s^{-1}$ for GdFeFe[5] et de 45 $mM^{-1}.s^{-1}$ for GdFeFe[10] very close to the values found in Table 1.

This good agreement shows that our approach is very consistent to assess and decorrelate both contributions, and that indeed all the four samples have a constant value per Gd^{III} around 40 $mM^{-1}.s^{-1}$.

Figure S11
T_1-weighted MR images recorded under a field of 7 T and at 37°C with a spin-echo sequence (T_R = 22 ms and T_E = 3 ms)

a) GdFeFe[5]@$(dextran)_{25}$ phantoms at different concentration of Gd^{III}

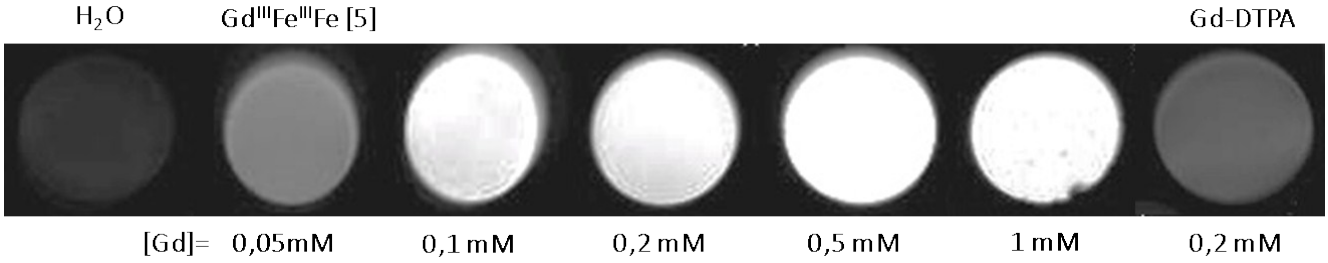

b) GdInFe[5]@$(dextran)_{25}$ phantoms at different concentration of Gd^{III}

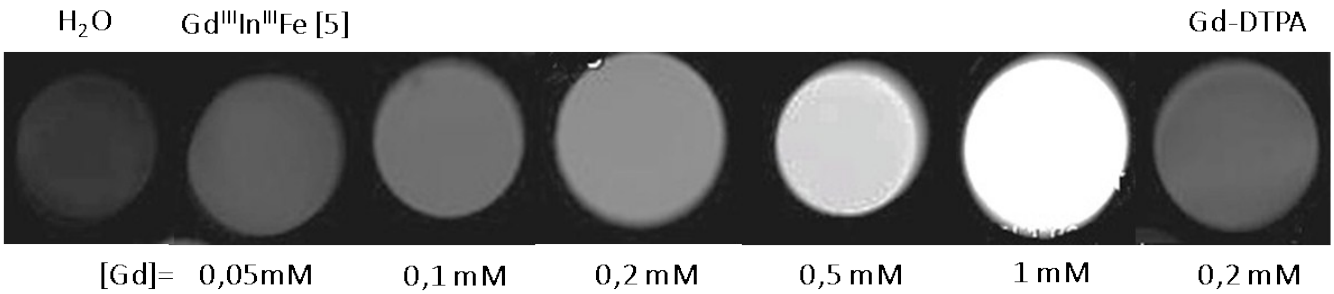

Figure S12
NMRD profiles of longitudinal relaxivity r_1 at 37°C- Comparison between particles GdFeFe [5] coated with dextran and PVP

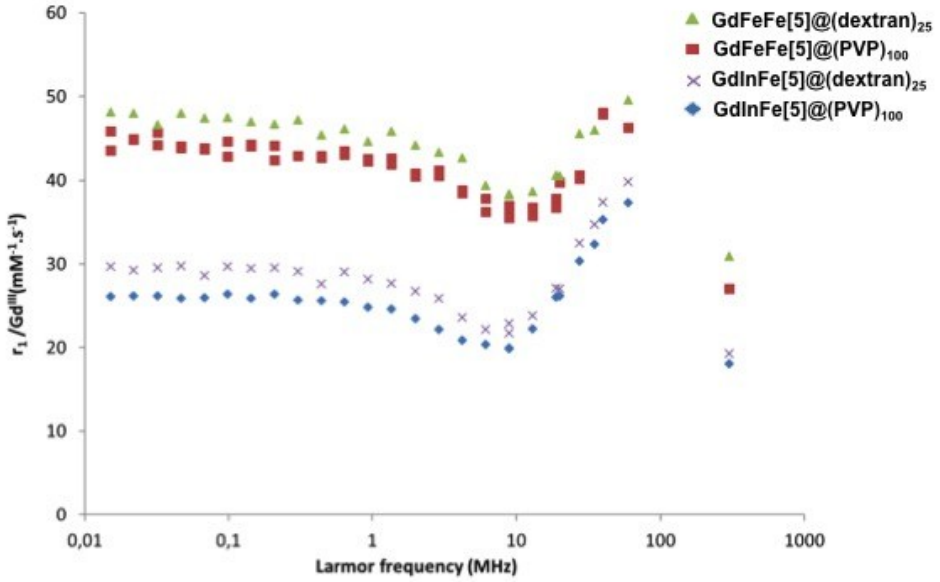

Figure S13
Cell viability measured on U87-MG cells after 24h of incubation

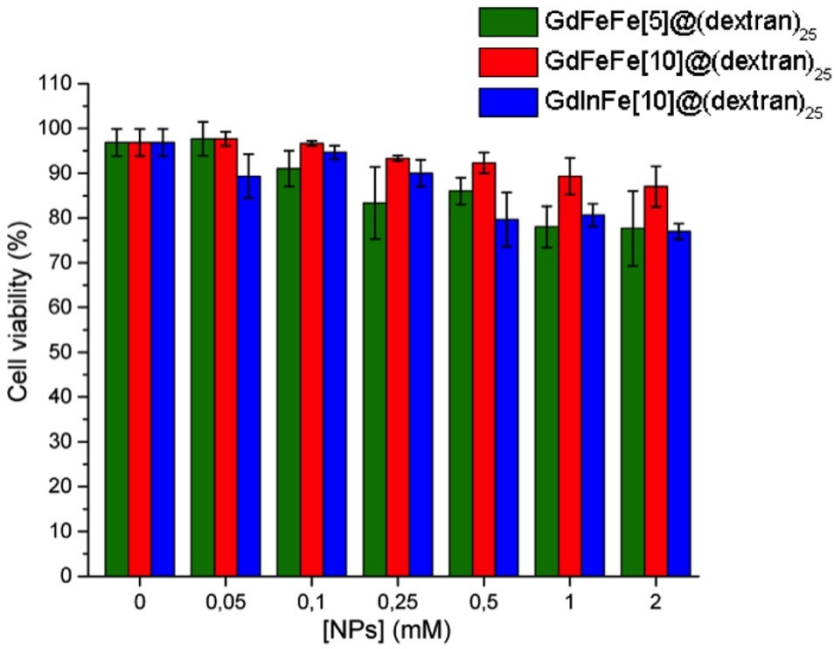

Cell viability

Human glioma U87-MG cells were cultured in 96-well plates one day before the experiment in DMEM containing 10% FBS, and non-essential amino acids, at 37°C 5% CO_2. The nanoparticles were added in the wells in culture medium for another 24-hour at the indicated concentration (n=3/condition) from 0.05 to 2 mM. Then, the cells were washed carefully with PBS, and incubated with Trypan blue 4% before manual counting. A minimum of 200 cells / well were counted. This method was used to avoid interferences with the strong color of the particles that may still attached to the cells after washing.

In vivo photothermal and photo-acoustic experiments

in vivo tumor model

A mouse bearing a subcutaneous CT26 tumor was sacrificed, the tumor was resected, placed into DMEM culture medium and cut into 20-30mm^3 fragments. These fragments were evaluated to contain approximately $9x10^5$ tumor cells, using hemocytometer measurement after trypsin disaggregation. The tumor fragments were transferred into sterile phosphate buffer saline (PBS) and inserted subcutaneously using a 12 gauge trocar (38mm) into the flank BALB/C mice previously disinfected with alcohol.

Photothermal therapy

On day 6 after implantation tumors were injected with 50 µL of GdFeFe solution at a concentration of 500µg/mL, controls tumors were injected with PBS. Tumors were then irradiated with an 808 nm at 1 Wcm^{-2} for 3 minutes. The tumor surface temperature was controlled using an infrared thermal camera (FLIR SC7000, FLIR Systems Inc.).

Photoacoustic Imaging

To evaluate the PAI contrast efficiency of GdFeFe, 25 µg were injected into CT26 tumors. All mice were anesthetized with gaseous anesthesia (isofluorane/air 4% induction and 1.5% during imaging) during the procedure according to ethical animal treatment procedures. Mice were scanned with a PA system (VeVo ® LZR SW2.2.0, VisualSonics, Inc., FUJIFILM, Institut Jacques Monod, Université Sorbonne Paris Cité, Paris, France) at different time intervals using a linear array transducer LZ550 (36 MHz center frequency, 32-55 MHz band width, 44µm axial resolution, 14 x 15 mm2 image size) previous and after injection to obtain PA images. The 3D B-mode and PA spectroscopic scans at 808nm were performed on the subcutaneous tumors. Images were analyzed using VeVo®Lab software (Visualsonics, Canada).

Figure S14

Infrared camera images (showing temperature increase in the tumor)

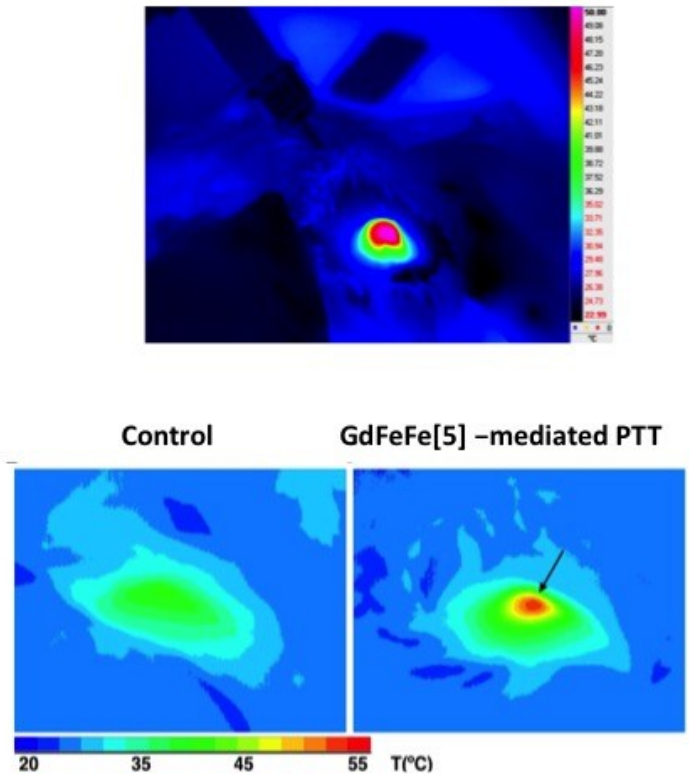

The high temperature increase of 50°C observed on the very central part of the tumor may be accompanied by some heating of surrounding normal tissue and it may possible that not only tumor cells will be affected. However, the "normal" cells within the tumor tissue are part of the tumor microenvironment and many of them such as cancer-associated fibroblasts or tumor-associated macrophages have demonstrated to favor tumor development, therefore affecting these cells during the process of PTT would contribute to the induction of a tumor regression.

Photoacoustic image at 808 nm at different stages of injection

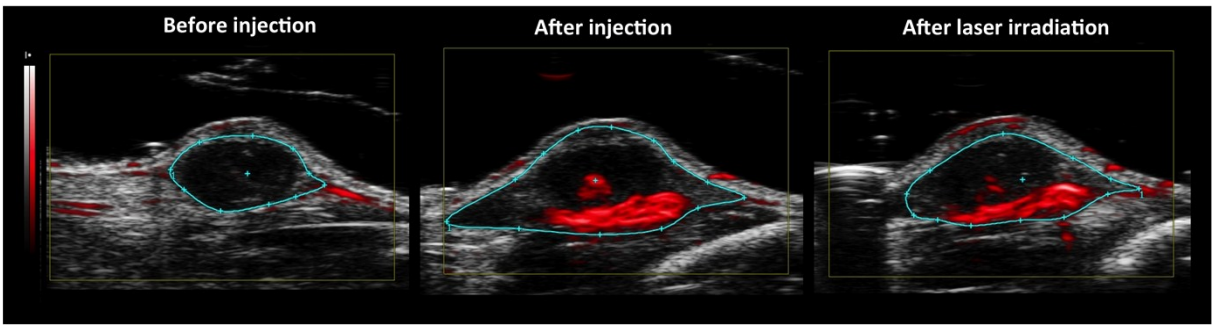

Evolution of weight of mice with time

Mice	Sample	Day 0	Day 5	Day 9	Day 13
1	PB	20,4	19,5	19,8	20
2	PB	18,8	19,2	19	18,7
3	PB	18,4	19,2	19,5	20
4	PB	18,5	18,1	18,6	19,7
5	PB	19,4	19	19,8	20,2
16	PB	16,1	15,6	15,5	15,4
7	Control	18	19,2	19	19,2
8	Control	19,2	19,9	19,8	21,9
6	Control	19,1	19,7	19,9	20,3
9	Control	18,3	19,4	19,5	20,3

Fig S15: PTT in colloidal solution at different concentrations in GdFeFe[5]